

Materials Science, Mechanical Structures and Engineering

Edited by
Salmah Husseinayah

Materials Science, Mechanical Structures and Engineering

Edited by
Salmah Husseinayah

Materials Science, Mechanical Structures and Engineering

Selected, peer reviewed papers from the
2014 2nd International Conference on
Mechanical Structures and Smart Materials
(2nd ICMSSM 2014),
August 16-17, 2014, Kuala Lumpur, Malaysia

Edited by

Salmah Husseinayah



Copyright © 2014 Trans Tech Publications Ltd, Switzerland

All rights reserved. No part of the contents of this publication may be reproduced or transmitted in any form or by any means without the written permission of the publisher.

Trans Tech Publications Ltd
Churerstrasse 20
CH-8808 Pfaffikon
Switzerland
<http://www.ttp.net>

Volume 680 of
Applied Mechanics and Materials
ISSN print 1660-9336
ISSN cd 1660-9336
ISSN web 1662-7482

Full text available online at <http://www.scientific.net>

Distributed worldwide by

Trans Tech Publications Ltd
Churerstrasse 20
CH-8808 Pfaffikon
Switzerland

Fax: +41 (44) 922 10 33
e-mail: sales@ttp.net

and in the Americas by

Trans Tech Publications Inc.
PO Box 699, May Street
Enfield, NH 03748
USA

Phone: +1 (603) 632-7377
Fax: +1 (603) 632-5611
e-mail: sales-usa@ttp.net

Preface

Dear Distinguished Authors and Guests,

The Organizing Committee warmly welcomes you to the 2014 2nd International Conference on Mechanical Structures and Smart Materials (2nd ICMSSM 2014), held in Kuala Lumpur, Malaysia, August 16-17, 2014.

The topics of ICMSSM 2014 cover different areas of Mechanical Structures and Mechanical Engineering, Material Science and Engineering, Materials Manufacturing and Processing .The peer-reviewed, selected papers and additional lectures with breakthrough contributions enlighten the technical program. Apparently, the conference program is extremely rich, professional, and featured with high-impact. The aims of the conference therefore provide an excellent platform for participants to exchange and share new ideas and practical experiences, to establish business or research relations and to search global partners for future collaboration.

We earnestly hope that the conference proceeding can contribute and provide you for significant and improved knowledge in the contemporary scientific and material fields.

On behalf of the organizing committee, I would like to thank Anne, Tanja, Dorte and all the editors from Trans Tech Publications for their great support to ICMSSM 2014. Without their excellent editorial work, the proceedings of ICMSSM 2014 cannot be published so timely and successfully.

Finally we wish all the authors and attendees a unique, rewarding and enjoyable memory at the 2nd ICMSSM2014 in Kuala Lumpur, Malaysia. We look forward to your participation in the 3rd ICMSSM in 2015.

With our warmest regards,

Jenny Ji

Conference Organizing Chair

August 26, 2014

BOSI EDU

Committees and Sponsors

Editorial Chair

ASSOC. PROF. DR. SALMAH HUSSEINSYAH, Universiti Malaysia Perlis (UniMAP)

Conference Chair

Jenny Ji, BOSI Education & Consultancy, China

International Committee

Malaysia:

Dr.Chong Wen Tong, University of Malaya, Malaysia

Dr.Ching Yern Chee, University of Malaya, Malaysia

Dr.Nik Hisyamudin Muhd Nor, Universiti Tun Hussein Onn Malaysia, Malaysia

China:

Pak Kin WONG, University of Macau, Macau, China

Prof. Qingsong Xu, University of Macau, Macau, China

Prof. Ka-Veng YUEN, University of Macau, Macau, China

South Korea:

Prof. Sung-Hoon AHN, Seoul National University, South Korea

Canada:

Assistant Pro. Dr. M. Shahria Alam, The University of British Columbia, Canada

India:

Geetesh Goga, K.C. College of Engineering and I.T.Nawanshahr (Punajb), India

Table of Contents

Preface, Committees and Sponsors

Chapter 1: Materials Science

The Fuzzy Comprehensive Evaluation of 18Cr2NiWA's Cutting Processing Performance M.L. Gong, Z.Y. Huo and H.Y. Liu	3
Experimental Investigation on Compression and Chemical Properties of Aluminium Nano Composite B. Vijaya Ramnath, C. Parswajinan, C. Elanchezhian, S.V. Pragadeesh, C. Kavin, P.R. Ramkishore and V. Sabarish	7
Tensile Properties of Semi-Solid Die Cast AC4C Aluminum Alloy K.R. Shi, S. Wisutmethangoon, J. Wannasin and T. Plookphol	11
Hot Compression Deformation Behavior of Mg-Gd-Y-Zn-Zr Alloy G. Lu, Z.P. Xie, Z.M. Zhang, Y.B. Yang and B.C. Li	15
Investigation on Compression and Hardness Properties of Abaca and Manila Hybrid Composite V.M. Manickavasagam, B. Vijaya Ramnath, C. Elanchezhian, V. Vignesh, V. Vijai Rahul, S.U. Sathya Narayanan and V. Tamilselvan	23
Analysis of Mechanical Properties between Sugarcane Bagasse/LDPE Composites versus Coconut Coir Wax/LDPE Hybrid Composites K. Rassiah, P. Balakrishnan and K. Haron	27
Interaction of Purple Sweet Potato Extract with Ascorbic Acid in FeCl₃ Solution Ayende, A. Rustandi, J.W. Soedarsono, D. Priadi, Sulistijono, D.N. Suprpta, G. Priyotomo and R. Bakri	32
Time-Temperature Effect for Preparation of SnO₂ Nanostructures Using Carbon Assisted D. Polsongkram, P. Chamninok, S. Changsakul, A. Sriputhorn and S. Pukird	38
The Glucose-Responsive Nanogel Based on Phenylboronic Acid L. Zhao, L.Y. Wang and G.Q. Gai	42
The Glucose-Sensitive Nanocarrier Based on Phenylboronic Acid L. Zhao, L.Y. Wang and G.Q. Gai	46
Fabrication and Evaluation of Tensile Properties of Kenaf-Flax Hybrid Composite V.S. Srinivasan, S. Rajendra Boopathy and B. Vijaya Ramnath	50
Physical Properties and Microstructure of the Fly Ash Based-Geopolymer/Granule Composites J.H. Won and S.G. Kang	54
Effects of Bi³⁺ Doping Amounts on the Magnetic Properties of FeSmO₃ Nanopowders X.W. Liu, H. Liu, Y. Zhang and X.W. Qi	61
Effect of La-Zn Doping on Magnetic Properties of SrFe₁₂O₁₉ X.W. Liu, X. Chen, W.D. He and X.W. Qi	66
A Brief Review and Framework towards Synthesising Silicone-Hydrogel Materials that Mimic Skin Deformation Behaviour N.N. Azmi, I.I. Shahrul Azhar and J. Mahmud	70

Chapter 2: Material Properties and Processing Technologies

Grain and Feature Size Effect on Material Behavior for Micro-Sheet-Forming M.A. Musa, A.R. Razali and N.I. Kasim	77
The Development of Prefabricated Concrete Structures S.B. Liu and L. Duan	81
Investigation of Filtration of Aliphatic Base Oil with Vibratory Shear Enhanced Process in Mechanical Actions R. Cheraghi Kootiani, A. Farokhi Nejad and M. Pourasghar Lafmejani	85

Bond Strength Comparison between Silicon and Glass Based Surface Using Anodic Bonding M.H.A. Aziz, Z. Sauli, V. Retnasamy, W.M. Wan Norhaimi, A.K.T. Yeow and H. Kamarudin	89
Contact Angle Analysis on Glass Based Surface M.H.A. Aziz, Z. Sauli, V. Retnasamy, W.M. Wan Norhaimi, S. Taniselass and H. Kamarudin	93
Experimental Study on the Single-Sided Double-Point Resistance Welding of Bus Roof Skin H.B. Huang, J.C. Liu, X.L. Ke and X.H. Lin	97
Reflectance Analysis of Sputtered Indium Tin Oxide(ITO) Using UV Lambda Z. Sauli, V. Retnasamy, C.J. Keng, M. Palianysamy and H. Kamarudin	102
FPSO Underwater Mooring Line Breakage Analysis Based on Broken Wire Material Test Z. Xu and Y. Wang	106
Preliminary Study on Resistance of Non-Treated and Treated ITO Films Z. Sauli, V. Retnasamy, C.J. Keng, M. Palianysamy and H. Kamarudin	111
Research on Architecture Material Strength Measurement System Based on Ultrasonic Sensor Array R.F. Tao	115
Shape Memory Alloy Applications in Bone Fixation: State of the Art M.R. Hassan and Y.T. Haw	119
Experimental Cutting Force Properties on Interpenetrating Network Composites with Double Metal Phases N. Fan, Y. Yu and Y. Bai	123
Hydrophilicity Characterization on Cleaned Bonded Silicon Based Surface M.H.A. Aziz, Z. Sauli, V. Retnasamy, W.M. Wan Norhaimi, M. Mohamad Isa and H. Kamarudin	127
Surface Roughness and Grain Size Analysis of Treated Indium Tin Oxide(ITO)Film V. Retnasamy, Z. Sauli, S. Taniselass, N. Ahmad, C.J. Keng and H. Kamarudin	131
Properties of Special Mortar Made with Raw Waste Material M.S.H. Mohd Sani, F. Muftah, M.I. Ismail and M. Ab. Rahman	135
Effects of Patch Geometrical Parameters on Mechanical Properties of Damaged Metallic Structure Repaired with Adhesively Bonded Composite Patch K. Zhou, D. Zhang and H.D. Wang	140
Watermelon Rind: A Potential Adsorbent for Zinc Removal N. Othman, Y.S. Kueh, F.H. Azizul-Rahman and R. Hamdan	146
Zinc Removal Using Honey Dew Rind N. Othman, A.S. Che-Azhar and A. Suhaimi	150
Numerical Simulation and Experiment of Traveling Wave Piezoelectric De-Icing Technique Q.Y. Li, T. Bai and C.L. Zhu	154
Failure Analysis of Composite Laminates under Biaxial Tension: A Review and Framework M.D. Muhamad Irwan, M.A. Zurri Adam and J. Mahmud	160

Chapter 3: Applied Mechanics and Engineering Design

Study on Shallow Embedded Column Foot of Reactive Powder Concrete Pole Mechanical Properties Y.Z. Jia and J.L. Xu	167
Large Span Double Truss Lateral Stability Analysis Y.Z. Jia and Y.X. Wang	171
The Pole Design of 500kV Centrifugal Concrete Filled Thin-Wall Steel Tubular Structures Y.Z. Jia and C.H. Zhang	175
Review of Studies on the Seismic Behavior of Composite Shear Walls with Double Steel Plates and Filled Concrete Y.J. Zhang, W.X. Liu and X.S. Shao	179
Analysis on the Couple Field of Fixed Tube-Sheet Heat Exchanger Y.L. Xu, W.Y. Chen and Q.W. Yang	182
Aspects of Alternative Dispute Creating Bolted Joint Technology Flowdrill J. Mascenik and S. Pavlenko	186
Ground Movements in Shield Tunneling and Impacts on Railway Culvert Y.Z. Jia and R. Li	190

Parallel Green Design of Machine Product B. Zhang, T.H. Jiang and C.H. Chen	194
Research on Rolling Element Bearing Fault Diagnosis Based on EEMD and Correlated Kurtosis X.L. Wang, W.H. Han, H. Gu, C. Hu and X.X. Han	198
Flexural Capacity of Plate Girders with Corrugated Webs Strengthened with Angles S.H. Lho, M.W. Park, Y.K. Ju and S.D. Kim	206
Influence of Deformation of the Wheel Disk-Type Body on the Tooth Load Distribution over the Facewidth in Helical Gears M. Krasiński	210
Natural Frequencies of Functionally Graded Beams by the Various Shear Deformation Theories J. Wu and S. Xiang	216
The Analysis of Finite Element about the Interaction between Seasonal Frozen Soil and Tower Pile Foundation F.L. Gan and D. Zhao	220
An Experimental Study on the Cutting Forces, Surface Roughness and the Hardness of Al 6061 in 1D and 2D Ultrasonic Assisted Turning R. Nosouhi, S. Behbahani, S. Amini and M.R. Khosrojerdi	224
Finite Element Analysis for Petiole's Fracture of Mine-Used Explosion-Proof Axial Fan Z.L. Song, D.C. Xie and L.Y. Ou-Yang	228
Calculation of Torsional Stiffness of Conductor and its Influence on the Stability of Motion Z.H. Cheng and C. Zhang	233
Effect of Pressing Pressure on Density and Hardness of Powder Miscanthus Reinforced Brake Pads M. Unaldi and R. Kus	237
Comparative Analysis of Bearing Capacity of Inclined and Vertical Excavated Foundation R. Chen, H.F. Liu, D.X. Hao and Z.Y. Wang	241
A Framework for Experimental-Numerical Analysis of Woven Laminates Failure M.Z. Mohd Zairil Hafizi, M.D. Muhamad Irwan, M.A. Zurri Adam and J. Mahmud	245
The Finite Element Analysis on the Compression Splicing Position of Strain Clamp in Guy Tower Z.Q. Wang, J. Li, W.G. Yang and Y.F. Cheng	249
Study on Impact Characteristics of CFRP Structural Member According to Stacking Conditions J.H. Choi, Y.J. Yang, C.S. Cha and I.Y. Yang	254
Study on Random Vibration Response Analysis for the Sphere Cylinder Assembly in Aerospace Vehicle D.L. Sun, Z. Zhao, K. He and R.D. Liao	258
Incremental Dynamic Analysis of Shape Memory Alloy Braced Steel Frames S. Moradi and M.S. Alam	263
Kinematics and Efficacy Analysis of the Seni Silat Cekak Malaysia (Kaedah A) G. Mustapha, W.R. Wan Sulaiman, A.P.P. Abdul Majeed, N.H. Mohd Yahya and J. Mahmud	267
Research on Piezoelectric Micropump of Combination of Active and Passive Valves J. Sun, P. Zeng and H.L. Lu	271
Theoretical Modeling of Pressure Force for CFRP Laminated Plate Interference-Fit Joining P. Liu, K.P. Du and W.L. Li	276
Preliminary Numerical Analysis of a Platform Structure A.K. Sohaimi, A.P.P. Abdul Majeed and J. Mahmud	280
A Trigonometric Shear Deformation Theory for Free Vibration Analysis of Functionally Graded Plates J. Wu and S. Xiang	284
Development of Droplets Penetrating Roots Performance Test Device and Tests Applied this Device in Ultrasonic Aeroponic System Y. Teng, J.M. Gao and C.J. Liu	288
Simulation and Experimental Investigation of Springback in Air V-Bending Process Using Finite Element Method (FEM) M.S. Buang, S.A. Abdullah and J. Saedon	292

Chapter 4: Mechanical Engineering and Control Systems

Kinematics Modelling and Simulation of Aero-Engine Fuel Piston Pump J.F. Fu, H.C. Li, J. Li and S.H. Wang	299
A Design Method of Aero Fuel Centrifugal Pump with Integrated Inducer and Impeller J. Li, H.C. Li, J.F. Fu and S.H. Wang	303
Takeoff Performance Analysis Based on Aeroengine EGT Trend Monitoring and Control F. Qiang and F. Ding	307
Positional Accuracy Based on a Load Identification Optimization on a Linear Motor Sheet Forming Feeder N.I. Kasim, A.R. Razali and M.A. Musa	311
Dynamic Analysis and Balance Design for a Constant Temperature Oscillator Based on ADAMS Q. Tao, Z.H. Feng, M. Lei and Z.M. Wang	315
Determining the Energy-Optimal Base Position of Industrial Robots by Means of the Modelica Multi-Physics Language M. Gadaleta, A. Genovesi and F. Balugani	320
The Analysis of Displacements and the Load Distribution between Elements in a Planetary Roller Screw F. Lisowski	326
Punching Automatic Line Served by a Portal Robot P.C. Patic, L. Pascale and G. Măntescu	330
Research on Fuzzy PID Controller for AC Permanent Magnet Synchronous Motor Servo System H. Hu and Y.X. Cui	334
Development of the Electronic Control System for Air-Powered Engine P.L. Chen, F.Z. Deng, J. Xu and M.H. Liu	338
Research on the Model of Pneumatic Servo Mechanism Controlled by Pulse Width Modulation D.X. Zhang, Z. Yang and Z. Yang	342
Research of Subway Electro-Pneumatic Brake Force Distribution Strategies M.L. Wu, L.Z. Wu, Y.F. Li and C. Tian	347
Method of Numerical Simulation of a Centrifugal Separator for Cleaning Petroleum Products N. Vatin, D. Nemova and N. Kharkov	354

Chapter 5: Researches of Transmission Line Construction

Estimation of Uplift Capacity of Excavated Foundation of Transmission Lines D.X. Hao, Y.C. Gao and R. Chen	361
Nonlinear Analysis of 220 kV Power Transmission Tower and Gradient Optimization X.Z. Zhang and X.W. Wang	365
Application of Cement Soil Mixing Pile for Transmission Line Q. Xiao, B. Yan and G.L. Du	370
Fine Damage Identification Method of Transmission Tower Based on Concurrent Multi-Scale Modeling C.C. Liu, S.Y. Hou, W.Q. Li and Z.W. He	374
Research Status and Prospect of Transmission Tower Structure Damage Identification W.X. Liu, L. Lu and Z.C. Li	379
Multi-Scale Analysis of the UHVDC Transmission Tower C.C. Liu, W.Q. Li, S.Y. Hou, Z.W. He and F. Gao	383
Dynamic Simulation Analysis of Transmission Line Tension Stringing W. Kong, Y.B. Zhang and W.L. Peng	387
The Transmission Tower with Angles Composed by the Variable Cross-Section is Studied Modal Analysis and Secondary Stress L. Qin and G.R. Yu	391

The Life Prediction of Transmission Tower Based on Multi-Scale Analysis C.C. Liu, Z.W. He, Y.J. Pan, W.Q. Li and S.Y. Hou	395
Seismic Responses of Multiple-Circuit Transmission Tower-Line System W. Kong, S.G. Men and Y.F. Tao	399
Analysis of a Fractured Lightning Rod on a Tower Structure at a Substation R. Li, H.Y. Yu, L. Wang, L.F. Wang, Q. Yuan, Q.Y. Chen, M. Qian, J. Hong, C.M. Tian and Y.H. Sheng	403
UHV KZ185 Crossing Tower Stress Analysis W. Kong and L. Wu	410
The Advantage Analysis of Applying Steel Tube Tower in Large Span Engineering J. Gong and L.N. Wang	414
Application of Large Size and High Strength Angle in UHV Transmission Line Tower F.L. Gan and X. Wang	418
Semi-Active Control for Vibration of Transmission Tower-Line with MRD W. Kong, Y.F. Tao and S.G. Men	422
The Influence of Geometry of Pedestal Piles in Silt on Uplift Behavior D.X. Hao, J.Z. Zhang and R. Chen	426

Chapter 6: Civil Engineering and Information Technologies

Intrusion Detection for Universal Attack Mode Based on Linear Temporal Logic with Past Construct P.Z. Qiao, Y.R. Wang and Y.K. Zhao	433
Research on Green Machine Product Design Evaluate System Based on AHP L.T. Yang, B. Zhang and T.H. Jiang	437
A New Hybrid Algorithm of Trust Region Methods D.Q. Zhang, P.P. Zhou and Q.H. Zhou	442
Measurement System Analysis of VS Lite G. Mustapha, M.S.A. Shafie, N.H.M. Yahaya and J. Mahmud	447
A Novel Approach for Intrusion Detection Based on Model Checking Interval Temporal Logic with Past Construct P.Z. Qiao and W.J. Zhu	451
Semi-Parametric Statistical Model for Extreme Value Statistical Models and Application in Automatic Control Y. Han	455
Optimization of Microclimate in Residential Buildings D. Vuksanovic, V. Murgul, N. Vatin and V. Pukhkal	459
Exhibition Pavilions Car Showrooms Based on Translucent Structures: Providing Microclimatic Comfort for Clients V. Pukhkal, D. Stanojevic, V. Murgul and N. Vatin	467
Highly Compacted and Reinforced Soil Beds as an Efficient Method to Build Artificial Foundation Based on Weak Soils R. Usmanov, N. Vatin and V. Murgul	474
Uses of Glass in Architecture: Heat Losses of Buildings Based on Translucent Structures Y. Nikitin, V. Murgul, N. Vatin and V. Pukhkal	481
Autonomous Systems of Solar Energy Supply under the Weather Conditions of Montenegro V. Murgul, N. Vatin and E. Aronova	486
A Relation between Function and Architectural Form in the Observers Perception R. Alihodzic, V. Murgul and N. Vatin	494
Glazing Design for Exhibition Pavilions Based on Translucent Structures under Winter Conditions during Cold Periods D. Vuksanovic, Y. Nikitin, V. Murgul, N. Vatin and V. Pukhkal	499
Research on Industrial Exhibitions Architecture Y. Nikitin, V. Goryunov, V. Murgul and N. Vatin	504
The Method to Determine Sites and Facilities for Wind-Diesel Power Plants Construction P. Pilipets, N. Vatin and V. Murgul	510
Enumeration of System Efficiency into Tariff of Renewable Energy Objects V. Elistratov, I. Kudryasheva and J. Miroshnikova	517

Decentralized Ventilation Systems with Exhaust Air Heat Recovery in the Case of Residential Buildings	
V. Murgul, D. Vuksanovic, N. Vatin and V. Pukhkal	524
Centralized Natural Exhaust Ventilation Systems Use in Multi-Story Residential Buildings	
V. Pukhkal, N. Vatin and V. Murgul	529
Double Skin Facades in Energy Efficient Design	
M. Penić, N. Vatin and V. Murgul	534
Classification Modeling of Parts for Complex Machinery Product Based on Design Structure Matrix	
W.H. Wan, J. Xu, P.L. Chen and M.H. Liu	539
The Steel Reinforced Concrete Structure in Main Plant for Heat Supply	
Q. Xiao and Q.W. Wang	543
Hydropower Development and Prospects Analysis	
S.Q. Xu	547
Finite Element Analysis of Concrete Filled Double Skin Steel Tubes for Wind Turbine Tower	
W. Kong, H.L. Wang and Y. Cai	551
Security Design System of Prison Architecture Based on New Materials	
W. Lin	557
Finite Element Analysis for Ladle Apparatus of Casting Using Free-Mesh Method	
J.S. Lee and G.H. Jo	561
Application of Carbon Fiber Reinforced Plastic to Automotive Seat Frames	
K.J. Lee, J.H. Choi and S.W. Seon	566

CHAPTER 1:
Materials Science

The Fuzzy Comprehensive Evaluation of 18Cr2NiWA's Cutting Processing Performance

Min-li Gong^{1,a}, Zhi-yi Huo^{2,b*}, Hong-yan Liu^{1,c}

¹ Hengyang Finance Economics and Industry Vocational College, Hengyang, Hunan, China

² Xingtai Polytechnic College, Xingtai, Hebei, China

^axtwangqian01@163.com, ^bhuozhiyi@sohu.com, ^c39563742@qq.com

Keywords: 18Cr2NiWA; cutting performance; fuzzy comprehensive evaluation

Abstract. The evaluation of material cutting performance is a complicated and comprehensive process. Only by using the fuzzy comprehensive evaluation way can we get a satisfactory result. This essay, on the basis of fuzzy theory, illustrates the steps of fuzzy comprehensive evaluation, introduces the factors influencing 18Cr2NiWA's cutting processing performance, gives a fuzzy evaluation of the factors, and thereby successfully solves the problems regarding these multi-factors' decision and evaluation.

0 Introduction

We should consider all aspects of factors because the things have variety of attributes or are affected by many factors. Fuzzy comprehensive evaluation means to make decision and overall evaluation of factors affected objects or phenomena, it is a mathematical tool for fuzzy synthetic decision. ^[1]

1 The basic steps of fuzzy comprehensive evaluation

First, we should make a independent evaluation according to each factor, and then click the all factors comprehensive evaluation, which mainly comprises the following steps:

(1) Analysis of the influence of elements

The factor set refers to the various important factors affecting evaluation objects as a collection of elements, the commonly used U said, $U = (u_1, u_2, \dots, u_n)$.

(2) Determine the weight number

In order to reflect the importance of each factor, the factors of u_i should be given a corresponding weight a_i , the form by the weight set $A = (a_1, a_2, \dots, a_n)$ is called the weight number,

and each weight should satisfy the normalization, $\sum_{i=1}^n a_i = 1, a_i \geq 0$.

(3) Evaluation results

The judge may make the evaluation objects of all kinds of the total evaluation results of the set, usually expressed in V , $V = (v_1, v_2, \dots, v_m)$

(4) Single factor fuzzy evaluation matrix

We can separate from a factor to determine membership about the evaluation set elements and the alternative element set, first, we judge factor u_i included in the i according to the evaluation object, the j element of u_j evaluation factors on the u_i concentration of membership degree is r_{ij} ($0 < r_{ij} < 1$), the single factor evaluation is in R_i , $R_i = (r_{i1}, r_{i2}, \dots, r_{im})$, Then the single factor evaluation matrix is

$$R = \begin{pmatrix} r_{11} & r_{12} & \dots & r_{1m} \\ r_{21} & r_{22} & \dots & r_{2m} \\ \vdots & \vdots & \vdots & \vdots \\ r_{n1} & r_{n2} & \dots & r_{nm} \end{pmatrix}$$

The single factor evaluation matrix can actually be regarded the fuzzy relation matrix between set of U and the alternative set of V , it is expressed as:

$$R_i = \frac{r_{i1}}{(u_i, v_1)} + \frac{r_{i2}}{(u_i, v_2)} + \dots + \frac{r_{in}}{(u_i, v_n)}$$

(5) Fuzzy comprehensive evaluation matrix

We must consider all of the influencing factors to obtain correct and comprehensive evaluation result, single factor fuzzy evaluation reflects only one of the factors that affect the evaluation object, so his will be through the fuzzy comprehensive evaluation in order to achieve the desired effect.^[2]

$$B = A \circ R = (a_1, a_2, \dots) \begin{pmatrix} r_{11} & r_{12} & \dots & r_{1m} \\ r_{21} & r_{22} & \dots & r_{2m} \\ \vdots & \vdots & \vdots & \vdots \\ r_{n1} & r_{n2} & \dots & r_{nm} \end{pmatrix} = (b_1, b_2, \dots, b_m)$$

2 The solution that meet the processing properties of materials and conform to fuzzy evaluation on 18Cr2Ni4WA

The cutting performance of the artifact material mainly depends on the material mechanics, physical properties (such as hardness, strength, ductility, toughness and thermal conductivity), the chemical composition and microstructure is the main factors affecting the mechanical, physical properties, so the machining properties of materials is not a single basic attribute, it is the comprehensive reflection of some basic properties of the material, rather than a comprehensive performance, we should use an index system and evaluation guidance not a single index.^[3]

The traditional methods for evaluating materials cutting performance mainly use the relative processing, such as:

- ① Tool life or cutting speed of the life;
- ② Cutting forces or cutting temperature;
- ③ Surface quality;
- ④ The difficulty level of chip breaking.

In fact, those are some fuzzy concept no absolute boundaries, such as a material easy cutting, easier cutting or hard cutting, there are many fuzzy in the evaluation of Material cutting performance. Moreover, we only use fuzzy comprehensive evaluation to evaluate the processing performance of material in order to get the convincing results, because the evaluation of processing performance of materials is a complex and comprehensive process.^[4]

18Cr2Ni4WA can be used in the case of tempering treatment but no carbonization, it belongs to the common low carbon alloy steel, high strength and good hardenability. The mechanical factors affecting the cutting performance: hardness, tensile strength, elongation, impact toughness, thermal conductivity, the physical and mechanical properties of the material are shown in table 1.

Tab.1 Physical and mechanical properties of 18Cr2NiWA steel

material type and grade	Hardness (HBS)	tensile strength (GPa)	impact toughness (MJ/mm ²)	thermal conductivity (W/mK)	Elongation (δ%)
18Cr2NiWA	359	1.13	1.17	41.22	11

(1) Establishing factor set

The physical and mechanical properties of table 1 are seen as factors lumped elements. u_1 is hardness, u_2 is hardness, u_3 is elongation, u_4 is impact toughness, u_5 is thermal conductivity, $U = (u_1, u_2, u_3, u_4, u_5)$.

(2) Build the weight set

The weight of each factor is one of key comprehensive evaluation, normally, we will carry out a unified treatment for expert review and production experience. the influencing of the strength and hardness are more important in the cutting performance rather than the impact toughness and impact of thermal conductivity, the weight set is A , $A = (0.30, 0.3, 0.1, 0.1, 0.2)$.

(3) Establishing choice set

Machining properties of materials can be divided into ten grades, as shown in table 2.

Tab.2 The scale of material cutting performance

cutting performance	easy cutting		more easy to cut		hard cutting		more difficult to cut				
class code	0	1	2	3	4	5	6	7	8	9	10
hardness (HBS)	50	100	150	200	250	300	350	400	480	635	635
tensile strength (GPa)	0.196	0.44	0.589	0.785	0.981	1.18	1.37	1.57	1.77	1.96	2.45
Elongation (δ%)	10	15	20	25	30	35	40	50	60	100	100
impact toughness (MJ/mm ²)	0.196	0.392	0.589	0.785	0.981	1.37	1.77	1.96	2.45	2.40	-
thermal conductivity (W/mK)	293	167	83.7	62.8	41.9	23.5	25.1	16.7	8.37	8.37	-

The ten level as alternative factors and it is expressed as $V = (v_1, v_2, v_3, v_4, v_5, v_6, v_7, v_8, v_9, v_{10})$.

(4) The results of fuzzy comprehensive evaluation

We can get the fuzzy matrix by calculating the degree of membership when the normal distribution curve as the membership function relationship.

$$R = \begin{pmatrix} 0 & 0 & 0 & 0 & 0 & 0.57 & 1 & 0.97 & 0.89 & 0.74 \\ 0 & 0 & 0 & 0.69 & 1 & 0.95 & 0.82 & 0.71 & 0.63 & 0.57 \\ 0 & 0.12 & 1 & 0.73 & 0.55 & 0.42 & 0.36 & 0.31 & 0.27 & 0.22 \\ 0 & 0 & 0 & 0 & 0 & 0.73 & 1 & 0.85 & 0.66 & 0.60 \\ 0 & 0 & 0.24 & 0.48 & 0.64 & 0.96 & 1 & 0.53 & 0.14 & 0.57 \end{pmatrix}$$

Fuzzy comprehensive evaluation is $B = A \circ R$, we can carry out fuzzy evaluation by using $M(\circ, +)$ model according to the specific situation, therefore the following formula is true.

$$\begin{aligned}
 B &= A \circ R \\
 &= (0.3 \quad 0.3 \quad 0.1 \quad 0.1 \quad 0.2) \circ \\
 &\left(\begin{array}{ccccccccc}
 0 & 0 & 0 & 0 & 0 & 0.57 & 1 & 0.97 & 0.89 & 0.74 \\
 0 & 0 & 0 & 0.69 & 1 & 0.95 & 0.82 & 0.71 & 0.63 & 0.57 \\
 0 & 0.12 & 1 & 0.73 & 0.55 & 0.42 & 0.36 & 0.31 & 0.27 & 0.22 \\
 0 & 0 & 0 & 0 & 0 & 0.73 & 1 & 0.85 & 0.66 & 0.60 \\
 0 & 0 & 0.24 & 0.48 & 0.64 & 0.96 & 1 & 0.53 & 0.14 & 0.57
 \end{array} \right)
 \end{aligned}$$

The cutting performance of 18Cr2NiWA quenched and tempered steel belongs to grade 6 according to the principle of maximum membership $\max(b_i) = b_7 = 0.882$, it is very difficult to cutting steel.

We had a cutting test for any three of steels to validate determination results, the optimal cutting parameters obtained are shown in table 3.

Tab.3 The results of cutting test

workpiece material	cutting speed (mm/s)	cutting feed (mm)	cutting depth (mm)
38CrMnAl	2.25	0.27	2
38CrMnSi	2.55	0.20	2
18CrNi4WA	2.10	0.30	2

The three kinds of steel with the cutting performance of similar are hard to be cut, and the experimental results show that the method has higher accuracy. ^[5]

3. Conclusion

Usually, the evaluation of objective things or phenomena that is a procession composed of multi factors identification and evaluation. Fuzzy comprehensive of evaluation mathematics can solve the decision making problem of multi factors. In order to determine the amount of cutting and other processing parameters, we can accurate and comprehensive evaluation of machinability through fuzzy comprehensive evaluation, even though many important factors influence processing performance of mechanical cutting, and determine the amount of cutting and other processing parameters. Allocation of weight has certain subjectivity in the process of evaluation. we can hire experts and technical personnel to discuss in order to reduce man-made factors on evaluation.

Referances

- [1]Liu Yangsong, in: The fuzzy method of mechanical design, Machinery Industry Press (2012).
- [2]Chen Shufa,Application of fuzzy comprehensive evaluation in the selection of component materials,J. Machine design and research,Shanghai,1(2011)78-79.
- [3]Cao Yuge, in: Mechanical fuzzy reliability design, Machinery Industry Press (2011).
- [4]Huang Hongzhong, in: Fuzzy mechanical science and technology---An important development direction of mechanical science twenty-first Century,J.Chinese Journal of Mechanical Engineering,Beijing,3(2011)55-57.
- [5]Xie Qingsheng, in: Fuzzy optimization method for Mechanical Engineering, Machinery Industry Press (2010).

Experimental Investigation on Compression and Chemical Properties of Aluminium Nano Composite

B. Vijaya Ramnath^{1,a}, C. Parswajinan^{2,b}, C. Elanchezhian^{3,c},
S. V. Pragadeesh^{4,d}, C. Kevin^{5,e}, P. R. Ramkishore^{6,f}, V. Sabarish^{7,g}

vijayaramnathb@gmail.com, parswajinan@gmail.com

^{a,c} Professor, Department of Mechanical Engineering, Sri Sai Ram Engineering College, Chennai, Tamil Nadu, India- 600 044

^b Research Scholar, Department of Mechanical Engineering, SCSVMV University, Kancheepuram, Tamil Nadu, India- 631561

^{d,e,f,g} Department of Mechanical Engineering, Sri Sai Ram Engineering College, Chennai, Tamil Nadu, India- 600 044

Keywords: Aluminium, Carbon Nanotubes, Mechanical Testing.

Abstract:

Aluminium metal matrix composites are being widely investigated with Carbon Nanotubes (CNTs) as one of their reinforcing agents. This is done in order to improve the mechanical strength of the composite. Various studies on this concept have already been recorded. In this study, Aluminium has been reinforced with CNTs using powder metallurgy technique. The powders of aluminium and CNT are ball milled, compacted in a die made up of die steel, and then sintered. The specimens thus obtained were subjected to hardness, compression and chemical tests and the values were compared with pure aluminium specimen fabricated by same technique. The study indicated that there was no improvement in hardness of the composite on addition of CNT. The compressive strength of the composite was increased by 143.58 MPa. The microstructure of pure aluminium and Al-CNT composite had fine grains of pure aluminium particles and Al-Si eutectic particles throughout the matrix phase.

1. Introduction:

Due to the exceptional physical and chemical properties, Carbon Nanotubes (CNTs) are being used as one of the reinforcing agents in Metal Matrix Composites (MMCs). CNT had already been reinforced with many metals in preparing metal matrix composites and had been tested. Aluminium is one of the most tested material reinforced with CNT. This is because aluminium has a higher strength at a lower weight and it is also easily available. Many studies have been previously recorded involving Al and CNT. Mina M.H. Bastwros et al. (2013) concluded that, when the CNT content was varied from 0wt% upto 5wt%, a significant increase in the hardness and the wear resistance, as well as a decrease in the coefficient of friction was observed. Jinzhi Liao and Ming-Jen Tan [4] observed that Small addition of CNTs (0.5 wt.%) resulted in the increase in tensile strength and hardness of the composite by comparing with the pure matrix. A.M.K. Esawi et al. (2010) observed that, Mechanical properties were found to improve significantly with the increase in CNT content and either exceeded or were close to predicted values based on composite theory except at 5 wt.% when the mechanical properties fell short of predicted values. Dominique Poirier et al. (2009) observed that, When milling the Carbon Nanotubes with the Aluminium, it undergoes grain refinement, and experiences an increase in lattice strain and results in formation of dispersoids. Thus an increase in the strength of Al matrix is expected. A.M.K. Esawi et al. (2009) determined that the tensile testing fracture surfaces of specimen showed uniform dispersion and alignment of the CNTs in the aluminum matrix but also showed CNTs acting as nucleation sites for void formation during tensile testing. D.-S. Lim et al. (2005) stated that when the

CNTs are added up to 12 wt.%, the wear loss decreased significantly and the friction coefficients were maintained same. H.J. Choi et al. (2010) observed that, as the grain size is reduced to ~ 150 nm and MWCNT volume increases up to 4.5 vol.%, yield stress notably increases and hence wear resistance is significantly enhanced in the specimen.

2. Experimental Setup:

2.1 Materials Used:

Aluminium and CNT powders are used as materials in this study. The aluminium powders used are of 99.5% purity with a mesh size of 200. The melting point and density of aluminium powders are 660°C and 2.70 g/cm^3 respectively. The properties of MWNTs used include purity $> 95\%$ on trace metal basis, melting point of $3652\text{-}3697^{\circ}\text{C}$, density of $\sim 2\text{ g/cm}^3$ and dimensions of 10-30 nm of outer diameter, 2-6 nm of inner diameter and 15-30 μm of length. As per TEM analysis, the impurities present in the MWNTs used are amorphous carbon of about $< 3\%$.

2.2 Specimen Preparation:

Powder metallurgy technique was used to fabricate the test specimens in this study. Initially, the aluminium powders and CNT were blended by ball-milling process for 30 min using steel balls of 5 mm diameter in a 250 ml steel jar maintaining the ball to powder weight ratio as 10:1 at 400 rpm. For compaction the powders, the powders were loaded into the die and punch set of 20 mm diameter and 60 mm height. A compacting load of 150 kN was applied using Universal Testing Machine (UTM) and the compacted green component had an height of 20 mm. the green component was then sintered in a muffle furnace from 300°C to 550°C . The sintering operation was done by increasing 100°C after one hour and at a rate of 50°C per hour after first hour. Sintering was done in order to convert the mechanical bonds formed by compaction into metallic bond, which adds strength to the component.

3. Results and Discussion:

In this study, hardness, compression and chemical tests were carried out for various specimens prepared above and the values were compared with that of pure aluminium specimen manufactured by same technique. Hardness of the specimen was found by applying a load of 1 kg in Vicker's hardness testing machine for both the samples. Addition of CNT did not show any significant improvement in hardness of the composite. The hardness of pure aluminium was found to be 46 HV and that of Al-CNT was found to be 45.6, 46.7, 48.2 HV and 45.8, 46.2, 47.6 HV respectively as shown in Table 1. The hardness between Al and Al-CNT are compared and shown in the figure 1.

Table 1. Hardness Test Result

Specimen	Hardness (HV)			
	Trial 1	Trial 2	Trial 3	Average
Al	48.8	47.7	48.8	48.43
Al-CNT	49.2	49.3	49.2	49.23

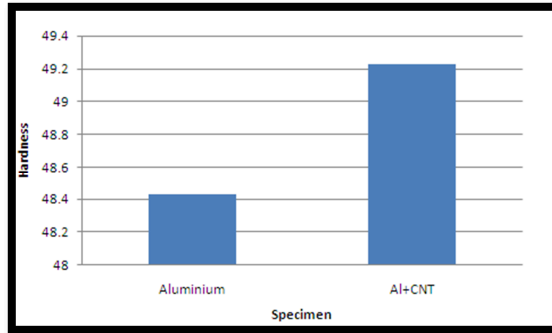


Fig 1. Comparison of Hardness of Al and Al-CNT

The pure aluminium sample withstood a load of 104.84 kN during compression test giving a compressive strength of 317.64 MPa. On the other hand, the Al-CNT specimen withstood a load of 150.75 kN giving a compressive strength of 461.22 MPa as shown in Table 2.

Table 2. Test Result of Compression test

Test	Trial	Al	Al-CNT	% Increase
Compressive Strength (MPa)	Trial 1	324.81	483.61	48.89
	Trial 2	328.81	493.26	50.01
	Trial 3	331.86	499.76	50.59

For chemical test, the microscopic structures of both the samples were analyzed using a metallurgical microscope. For a better view of grain structure under the microscope, 1% hydrogen fluoride (HF) solution was as etching agent. The test results thus obtained showed that in both the specimens, there appeared to be fine grains of aluminium particles with some Al-Si eutectic particles throughout the matrix.

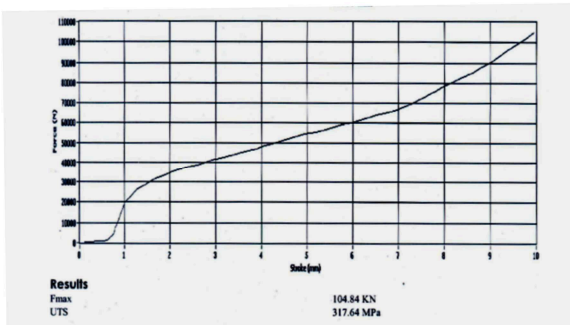


Fig 2. Applied Load vs Stroke for Aluminium

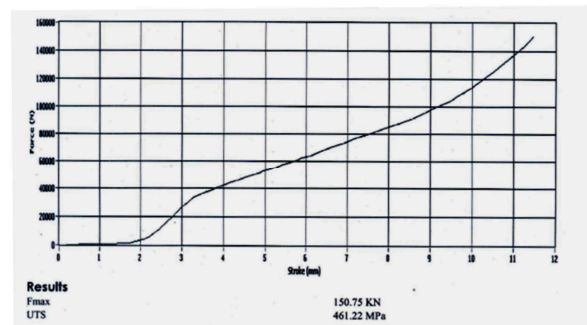


Fig 3. Applied Load vs Stroke for Al-CNT

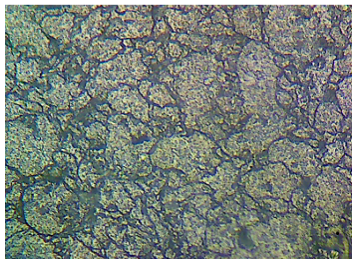


Fig 4. Microstructure of aluminium at 500x magnification.

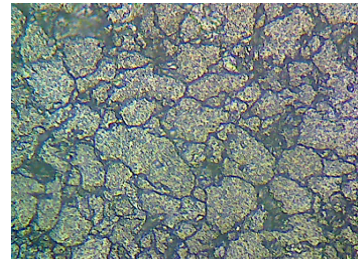


Fig 5. Microstructure of Al-CNT specimen at 500x magnification.

The graphs between applied load and stroke for Al and Al-CNT are shown in the figure 2 and figure 3 respectively. The microstructure of Al and Al-CNT specimen at 500x magnification are shown in the figure 4 and figure 5 respectively.

4. Conclusion:

To summarize, aluminium powders reinforced with CNT were fabricated in this study by using powder metallurgy technique and mechanical and chemical tests were carried out. The results were compared with pure aluminium specimen fabricated by same technique. The results are as follows:

1. Both the samples had nearly the same hardness values concluding that addition of CNT did not have any significant improvement in hardness value.
2. Compressive strength of the sample was found to be improved on addition of CNT. The compressive strength of unreinforced sample was 317.64 MPa and that of Al-CNT sample was 461.22 MPa.
3. Both the samples contained fine grains of aluminium particles along with some Al-Si eutectic particles throughout the matrix.

REFERENCES

- [1]. A.M.K.Esawi, K.Morsi, A.Sayed, M.Taher,S. Lanka,: “Effect of carbon nanotube (CNT) content on the mechanical properties of CNT-reinforced aluminium composites” -Composites Science and Technology 70 (2010) 2237–2241.
- [2]. H.A. Al-Qureshi, M.R.F. Soares, D. Hotza, M.C. Alves, A.N. Kleina, “Analyses of the fundamental parameters of cold die compaction of powder metallurgy”- Journal of Materials Processing Technology 199, (2008), 417–424.
- [3]. Mehdi Rahimian, NaserEhsani, Nader Parvin, Hamid rezaBaharvandi, “The effect of particle size, sintering temperature and sintering time on the properties of Al–Al₂O₃ composites, made by powder metallurgy”- Journal of Materials Processing Technology 209, (2009) 5387–5393.
- [4]. Jinzhi Liao , Ming-Jen Tan, “Mixing of carbon nanotubes (CNTs) and aluminum powder for powder metallurgy use”- Powder Technology 208 (2011) 42–48.
- [5]. Mina M.H.Bastwros, AmalM.K.Esawi, AbdallaWifi, “Friction and wear behavior of Al–CNT composites” Wear 307(2013)164–173
- [6]. Dominique Poirier, Raynald Gauvin, Robin A.L. Drew, “Structural characterization of a mechanically milled carbon nanotube/aluminum mixture”, Composites: Part A, 40, (2009), 1482–1489.
- [7]. A.M.K. Esawi, K. Morsi, A. Sayed, A. Abdel Gawad, P. Borah, “Fabrication and properties of dispersed carbon nanotube–aluminum composites”, Materials Science and Engineering: A Volume 508, Issues 1–2, 20 May 2009, 167–173
- [8]. D.-S. Lim, D.-H. You, H.-J. Choi, S.-H. Lim, H. Jang, “Effect of CNT distribution on tribological behavior of alumina–CNT composites”, Wear 259, (2005), 539–544.
- [9]. H.J. Choi, S.M. Lee, D.H. Bae, “Wear characteristic of aluminum-based composites containing multi-walled carbon nanotubes”, Wear 270, (2010) 12–18

Tensile Properties of Semi-Solid Die Cast AC4C Aluminum Alloy

Keren Shi^{1,2,a}, Sirikul Wisutmethangoon^{3,b}, Jessada Wannasin^{2,c}
and Thawatchai Plookphol^{2,d}

¹State Key Laboratory Cultivation Base of Natural Gas Conversion,
Ningxia University, Yinchuan 750021, China

²Department of Mining and Materials Engineering, Faculty of Engineering,
Prince of Songkla University, Hat Yai 90112, Thailand

³Department of Mechanical Engineering, Faculty of Engineering,
Prince of Songkla University, Hat Yai 90112, Thailand

^ashikeren@163.com, ^bsirikul@me.psu.ac.th, ^cjessada@alum.mit.edu, ^dthawatchai.p@psu.ac.th

Keywords: AC4C; tensile properties; fracture; GISS; die casting.

Abstract. In this study, semi-solid Al-Mg-Si alloy (AC4C) was produced by using the Gas Induced Semi-Solid (GISS) die casting process. The tensile strength and ductility of the semi-solid die cast Al alloy (GISS-DC) after T6 heat treatment were investigated and compared with those of the conventional liquid die casting (CLDC). The microstructures of GISS-DC and CLDC observed by an optical microscopy were presented. The ultimate tensile strength (UTS) and yield strength (0.2% YS) of GISS-DC are compatible with those of the CLDC. However, the GISS-DC has better ductility than the CLDC, this may be due to the smaller and more globular primary α -Al phase and rounder shaped-Si particle microstructures presented in the GISS-DC. Common shrinkage pores and defects were also observed by SEM from the fracture surfaces of both alloys.

Introduction

Semi-solid metal (SSM) technology has been continuously developed to produce Al alloys with uniform microstructures and better mechanical properties for the automotive industry. There are two major processing types of SSM: thixocasting and rheocasting [1]. A lot of research works have been focused on SSM processing as a way to cast near-net-shape products [2]. Gas Induced Semi-Solid (GISS) technique which was invented by the Innovative Metal Technology (IMT) team at Prince of Songkla University, Thailand is a novel, simple, economical and efficient rheocasting process which has succeeded to produce globular structure in many alloys [3,4]. Although many previous research works were focused on the properties of GISS squeeze cast alloys [5,6], only a few on the properties of SSM alloy produced by using GISS die casting process. So, the purpose of this work was to investigate the tensile property and microstructures of the SSM Al-Mg-Si alloy (AC4C) produced by the GISS die casting.

Experiment

Materials. The chemical composition of AC4C aluminum alloy produced by the GISS die casting (GISS-DC) and the conventional liquid die casting (CLDC) was shown in Table 1. During the GISS-DC, the aluminum alloy was melted in a graphite crucible in an electric furnace at 680 °C before casting. Approximately 200 g of the melt was taken out from the crucible using a ladle cup. Then, the nitrogen gas was injected through a graphite diffuser into the ladle when the rheocasting temperature (RCT) of the melt was about 616 °C, for about 10 seconds to create a semi-solid slurry with a low solid fraction of about 10% [1]. The schematic diagram of the GISS process was shown in Fig. 1. The SSM slurry was transferred to the die casting machine and then poured into the shot sleeve for die casting. The temperature of shot sleeve and die was kept at 200 °C. The schematic diagram of

the GISS-DC process was illustrated in Fig. 2. For the CLDC process, the ingot of AC4C Al alloy was melted at 680 °C, then the melt was poured into shot sleeve for die casting.

Table 1 Chemical composition of GISS-DC and CLDC aluminum alloys

Elements	Si	Fe	Cu	Mn	Mg	Zn	Ti	Cr	Ni	Pb	Al
CLDC	7.543	0.456	0.063	0.063	0.381	0.088	0.016	0.014	0.010	0.004	Bal.
GISS-DC	7.996	0.488	0.063	0.039	0.364	0.089	0.014	0.014	0.009	0.003	Bal.

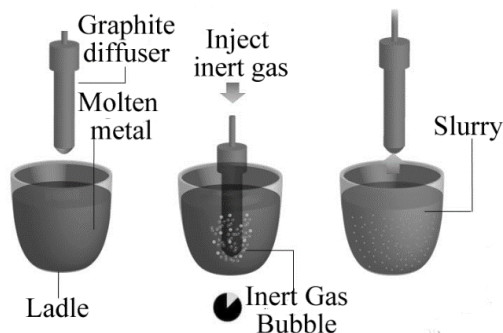


Fig. 1 Schematic diagram of GISS technique [7].

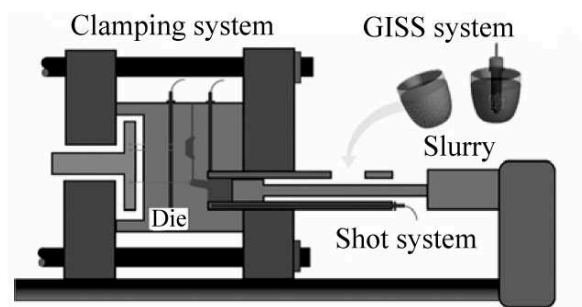


Fig. 2 Schematic diagram of GISS die casting process [8].

Tensile test. AC4C Al alloy produced by GISS-DC and CLDC were heat treated to T6 designation by a solution treatment at 540 °C for 4 h and artificially aged at 195 °C for 3 h after [3]. Tensile test was followed the ASTM E8-08 standard. Tensile specimens were prepared from GISS-DC and CLDC AC4C-T6 bars by machining. The dimensions of specimen were shown in Fig. 3. Tensile tests were performed in a universal testing machine, HOUNSFIELD Model H100KS, Serial No. 0068, using a constant cross-head speed of 1.5 mm/min, corresponding to a strain rate of $1 \times 10^{-3} \text{ s}^{-1}$.

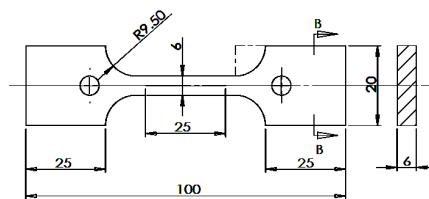


Fig. 3 Dimensions of tensile test specimen.

Results and Discussion

Microstructures. The microstructures of CLDC AC4C-T6 aluminum alloy (Fig. 4b) were composed of α -aluminum dendrites, eutectic silicon particles and Fe-bearing intermetallic compounds. While the rosaceous and globular primary α -aluminum phase and rounder shaped silicon particles were found in the GISS-DC AC4C-T6 (Fig. 4a).

Tensile test. The ultimate tensile strength (UTS), yield strength (0.2%YS) and elongation of the GISS-DC AC4C-T6 were compared with those of CLDC AC4C-T6 in Fig. 5, and listed in Table 2. At room temperature, the GISS-DC gained the UTS and 0.2% YS of 294.4 MPa and 241.5 MPa while the CLDC gained 298.2 MPa and 251.6 MPa, respectively. The averaged UTS and 0.2% YS of CLDC are slightly higher than those of GISS-DC. The elongation of GISS-DC and CLDC are 5.9% and

4.8%, respectively. The result shows that GISS-DC is more ductile than CLDC. This may be resulted from the fact that the GISS-DC microstructures are composed of smaller and more globular primary α -Al phase and rounder shaped-silicon particles when compared with the CLDC.

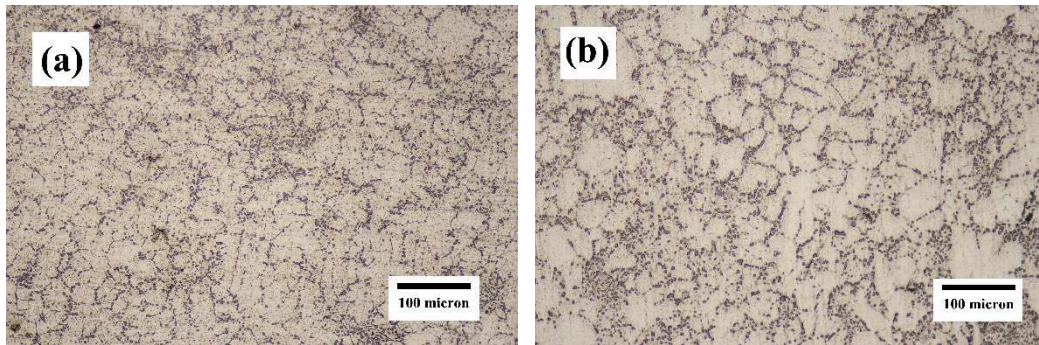


Fig. 4 Optical micrographs of (a) GISS-DC AC4C-T6 Al alloy and (b) CLDC AC4C-T6 Al alloy.

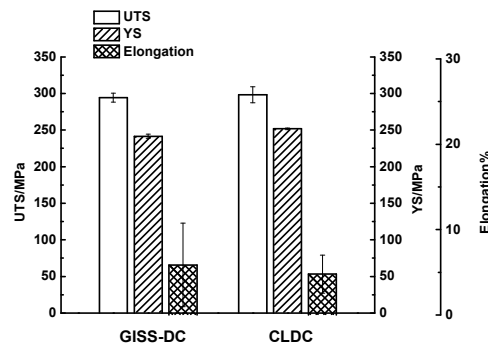


Fig. 5 Comparison of ultimate tensile strength (UTS), yeild stress (0.2% YS) and elongation of GISS-DC and CLDC AC4C-T6 aluminum alloys.

Table 2 Ultimate tensile strength (UTS), yield strength (0.2% YS) and elongation of GISS-DC and CLDC AC4C-T6 aluminum alloys.

Materials	UTS (MPa)	0.2%YS (MPa)	Elongation (%)
GISS-DC AC4C-T6	294.4±6.1	241.5±2.9	5.9±4.9
CLDCAC4C-T6	298.2±10.8	251.6±1.1	4.8±2.2

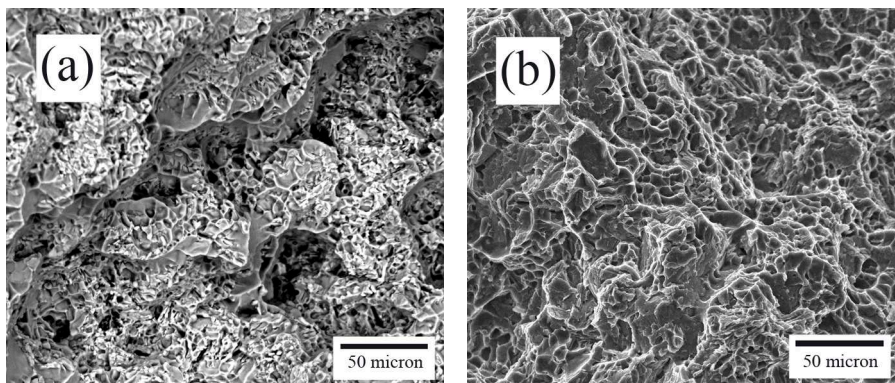


Fig. 6 SEM micrographs of fractured surfaces of (a) GISS-DC AC4C-T6 and (b) CLDC AC4C-T6 after tensile tests.

Fractography. The fractured surfaces of specimens after tensile tests were shown in Fig 6. At room temperature, both GISS-DC and CLDC AC4C-T6 were fractured in the brittle mode of quasi-cleavage form. The GISS-DC was more dimple structure. When the applied stress was increased, the internal stress was developed at Si particle and approached to its fracture stress, crack was initiated at the Si particle as observed on the fractured surface. Some common shrinkage pores and defects were also found in the fractures in both types of specimens.

Summary

1. The semi-solid AC4C aluminum alloy can be produced by using the GISS die casting process.
2. The UTS and 0.2% YS of both GISS-DC and CLDC are almost the same.
3. The GISS-DC gains more ductility than the CLDC. This may be resulted from the microstructures of GISS-DC, which are composed of smaller and more globular primary α -Al phase and rounder shaped-silicon particles.
4. Both GISS-DC and CLDC are fractured in the brittle mode of quasi-cleavage at room temperature.

Acknowledgement

The authors would like to thank the Department of Mining and Materials Engineering, Faculty of Engineering, Prince of Songkla University. The authors acknowledge the president scholarship from the President Office of Prince of Songkla University. This work was supported by the Higher Education Research Promotion and National Research University Project of Thailand, Office of the Higher Education Commission.

References

- [1] R. Burapa, S. Janudom, T. Chucheep, R. Canyook, J. Wannasin, Effects of primary phase morphology on mechanical properties of Al-Si-Mg-Fe alloy in semi-solid slurry casting process, *T. Nonferr. Metal. Soc.* 20 (2010) 857-861.
- [2] S. Tahamtan, M.A. Golozar, F. Karimzadeh, B. Niroumand, Microstructure and tensile properties of thixoformed A356 alloy, *Mater. Charact.* 59 (2008) 223-228.
- [3] J. Wannasin, R. Martinez, M. Flemings, Grain refinement of an aluminum alloy by introducing gas bubbles during solidification, *Scripta Mater.* 55 (2006) 115-118.
- [4] S. Wisutmethangoon, S. Thongjan, N. Mahathaninwong, T. Plookphol, J. Wannasin, Precipitation hardening of A356 Al alloy produced by gas induced semi-solid process, *Mat. Sci. Eng. A* 532 (2012) 610-615.
- [5] Q.G. Wang, Microstructural Effects on the Tensile and Fracture Behavior of Aluminum Casting Alloys A356/357, *Metall. Mater. Trans. A* 34 (2003) 2887-2899.
- [6] G. Ran, J.E. Zhou, Q.G. Wang, Precipitates and tensile fracture mechanism in a sand cast A356 aluminum alloy, *J. Mater. Process. Technol.* 207 (2008) 46-52.
- [7] T. Rattanochaikul, S. Janudom, N. Memongkol, J. Wannasin, Development of aluminum rheo-extrusion process using semi-solid slurry at low solid fraction, *T. Nonferr. Metal. Soc.* 20 (2010) 1763-1768.
- [8] J. Wannasin, S. Thanabumrungrul, Development of a semi-solid metal processing technique for aluminum casting applications, *Songklanakar J. Sci. Technol.* 30 (2008) 215-220.

Hot Compression Deformation Behavior of Mg-Gd-Y-Zn-Zr Alloy

Guang Lu^{1,a}, Zhiping Xie^{1,b}, Zhimin Zhang^{1,c*}, Yongbiao Yang^{1,d},
Baocheng Li^{1,e}

¹College of Materials Science and Engineering, North University of China, Taiyuan 030051, China

^axzp135464@sina.com, ^bforgexzp@163.com, ^cforgezzm@sina.com, ^dforgexy@sina.com,
^ewoddeyouxiang@163.com

Keywords: Mg-Gd-Y-Zn-Zr magnesium alloy; hot-deformation; flow stress; constitutive equation; dynamic recrystallization; deformation map

Abstract. The deformation behaviors of as-cast Mg-11Gd-2Y-Zn-Zr magnesium alloy were investigated by compression test with Gleeble-1500 thermal simulator at temperature of 623-753K and strain rate of 0.01-0.5 s⁻¹. The flow stress behaviors of the magnesium alloy were carried out at a strain of 0.7. The strain rate and deformation temperature had great influence on the flow stress behaviors. The flow stress increases with increasing strain rate and decreasing temperature. The flow stress has more than one peak stress at a strain rate of 0.5s⁻¹ showing continuous dynamic recrystallization (DRX) mechanism, while other flow stresses exhibited only one peak stress indicating discontinuous dynamic recrystallization (DDRX) mechanism. It was also found that the flow stress behavior could be described by the hyperbolic sine constitutive equation, in which the determined average activation energy is 273.426 kJ·mol⁻¹. The maximum error value between calculated value and experimental value is 5.5%. The deformation map was also established, and the best parameter for hot working was found to be 0.1s⁻¹/753k approximately.

Introduction

As a lightweight material with high specific strength and specific stiffness, Magnesium alloy has a great potential to be used for those applications such as automotive, aerospace, aeronautical, and electronic products[1-2]. It has been reported that rare earth elements could remarkably improve the mechanical properties of magnesium at room and high temperatures[3], which made the applications of magnesium alloy more attractive. In previous work, Rokhlin and Nikitina [4], and Kamado[5] developed Mg-10Gd-5Y-0.5Mn and Mg-10Gd-3Y-0.4Zr alloy, respectively, which had better performance and exhibited higher specific strength and creep resistance both at room and elevated temperature compare with that of conventional Mg alloys. These studies demonstrated brighter future applications of the magnesium alloy.

However, due to its low plasticity and formability owing to the hexagonal close-packed structure, the wrought magnesium alloys has not been applied broadly so far. So, it is a great challenge to explore the deformation characteristics and limits of magnesium alloys in order to provide optimized hot working parameters for the metal-forming industry.

Constitutive equation is one of the most useful tools for predicting the behaviour of material under given deformation conditions. The reliability of the output from constitutive equations depends to a large extent on the trustworthiness of input data. The necessary material data to build the equations in terms of relationships between flow temperature, stress, strain and strain rate could be received from consistent behaviour of deformation at a range of temperatures and strain rates on Gleeble-1500 thermal simulator.

The processing map based on the dynamic materials model (DMM) is considered to be an important model for optimizing the hot working parameters. By using the processing map, the plastic deformation mechanisms in various deformation conditions can be predicted, and the instable deformation zones could also be avoided during hot deformation process. The processing map based on DMM was established by Prasad and co-workers recently [6]. According to Prasad, the hot deformation work could be considered as power dissipater, And the total power P consists of

two complementary parts: G represents the power dissipation through plastic deformation, most of which are converted into heat, and J represents the power dissipation through microstructure transition. In this model, the content G and J are correlated by the parameter m (the strain rate sensitivity), which is defined as follows:

$$\left(\frac{\partial J}{\partial G}\right)_{\varepsilon, T} = \left[\frac{\partial(\ln \sigma)}{\partial(\ln \dot{\varepsilon})}\right]_{\varepsilon, T} = m \quad (1)$$

For an ideal linear dissipating body, $m=1$ and $J = J_{\max} = \sigma \dot{\varepsilon} / 2 = P/2$, and the power-dissipation capacity of the material can be estimated by the efficiency of power dissipation η , which is given by:

$$\eta = \frac{J}{J_{\max}} = \frac{2m}{m+1} \quad (2)$$

The instability map was developed on the basis of the extremum principles of irreversible thermodynamics applied for large plastic flow body. The onset of an instability criterion was defined below on the basis of power dissipation principles:

$$\xi(\dot{\varepsilon}) = \frac{\partial \ln(m/m+1)}{\partial \ln \dot{\varepsilon}} + m < 0 \quad (3)$$

The dependence of the instability parameter $\xi(\dot{\varepsilon})$ on temperature and the strain rate can be expressed by the instability map.

In recent years, many researchers focused on the rare earth magnesium alloys, such as Mg-Gd-Y-Zr[7] and Mg-Zn-Y-Zr[8]. But, the studies of Mg-Gd-Y-Zn-Zr magnesium alloys are quite limited and unclear. In this paper, to study the hot deformation behaviors and build constitutive equation and processing map, hot compression tests of Mg-11Gd-2Y-Zn-Zr alloy were conducted under different conditions. The processing of Mg-11Gd-2Y-Zn-Zr magnesium alloys could be guided from the constitutive equation and processing map in this experiment.

Experimental

The alloy has a composition of Mg-11Gd-2Y-Zn-Zr (wt%). The cast ingots were homogenized at 793K in a sulfur atmosphere for 4h followed by quenching into hot water. Cylindrical specimens for the compression tests were machined to 8mm in diameter and 12 mm in height utilizing electro-discharge machine. In order to decrease the friction and maintain uniform deformation, thin graphite sheets were placed between the compression specimen and the die during the test. Isothermal hot compression tests were performed on a Gleeble-1500D thermal mechanical simulator in the temperature range of 623–753 K and at strain rates of 0.001, 0.01, 0.1 and $0.5s^{-1}$ respectively. The specimen was induction heated at deformation temperature for 1 min and held for 3 min in order to obtain a stable and uniformity temperature prior to deformation. All specimens were compressed to a true strain of 0.7, and then water-quenched. Then, the specimens were cut symmetrically into two parts parallel to the compression axis. Center parts of the specimens were chosen as the investigation area of interest. Also, the regions vertical to the compression axis were the objects to be studied. After adequate grinding and polishing, specimens for optical observation were etched using solution of 4% HNO₃ with ethanol. An optical microscopy ZEISS Image A1m was used for microstructure observations.

Results and discussion

Microstructure of as-cast homogenized alloy. Fig.1 is the typical microstructures of the as-cast alloy with pre-homogenization. It could be seen that alloy structure was composed of primarily α -Mg matrix and eutectic β phase. The β phase formed by Mg-Gd-Y-Zn four elements precipitated as discontinuous network primarily at grain boundaries.

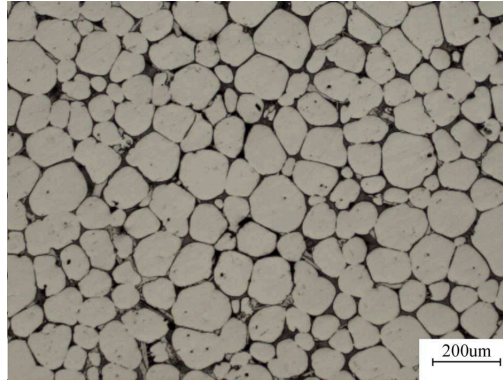


Fig.1 Microstructures of the pre-homogenized alloy

True stress—true strain curves. The typical true stress-true strain curves of homogenized magnesium alloy at different deformation temperatures and strain rates are presented in Fig.2.

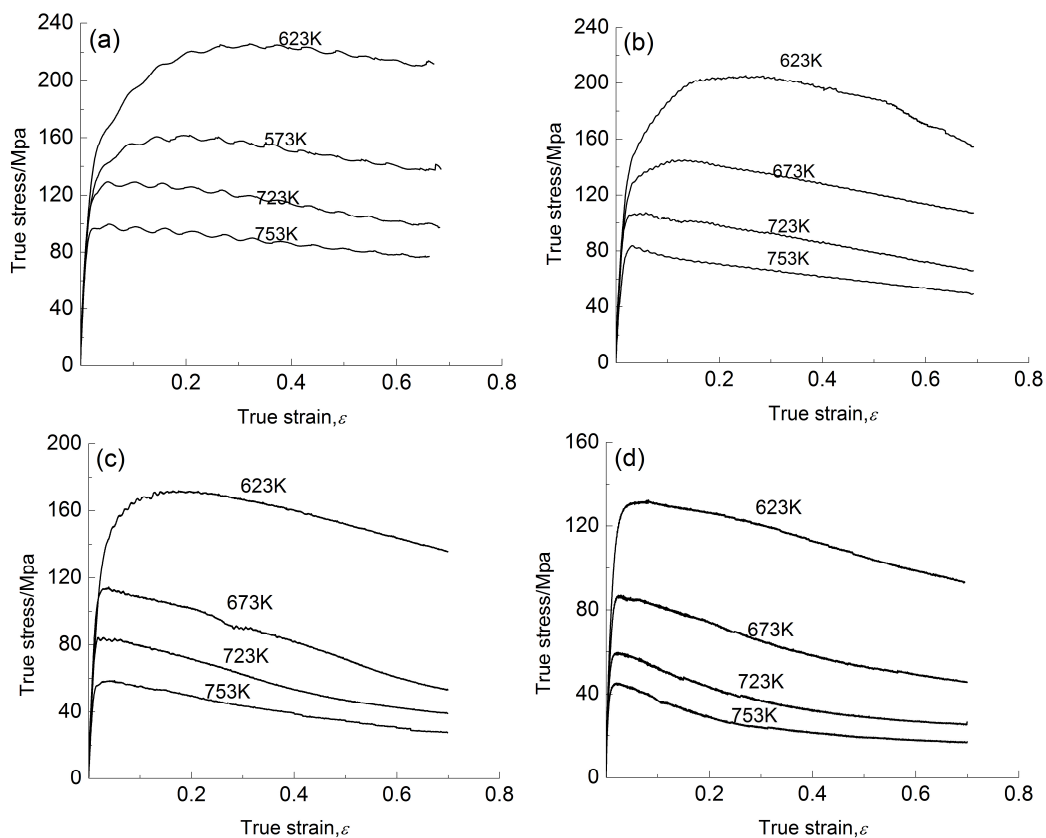


Fig. 2 True stress—strain curves of Mg-Gd-Y-Zn-Zr at various strain rates and deformation temperatures: (a) $\dot{\epsilon} = 0.5 \text{ s}^{-1}$; (b) $\dot{\epsilon} = 0.1 \text{ s}^{-1}$; (c) $\dot{\epsilon} = 0.01 \text{ s}^{-1}$; (d) $\dot{\epsilon} = 0.001 \text{ s}^{-1}$

Fig. 2 exhibits that flow stress diminishes with rising temperature and decreasing strain rate, especially at low temperature (573–623 K) and high strain rates (0.1–0.5 s^{-1}). At strain rate of 0.5 s^{-1} , more than one peak stresses were obtained on the flow stress. At other strain rates, the flow stress increased to a maximum value at first and decreased to a stable state finally. The curves showed different characteristics between two types of dynamic recrystallization mechanism: continuous

dynamic recrystallization (DRX) mechanism and discontinuous dynamic recrystallization (DDRX) mechanism[9]. One of the obvious differences between them was that the continuous DRX had only one peak stress, but DDRX had more than one peak stress. At the point of peak stress, the work hardening and softening reached balanced state and then the softening was more pronounced causing the stress to decrease.

Constitutive equation. The Arrhenius equation is widely used to describe the relationship among the strain rates, flow stress and temperature, especially at high temperature. Commonly, the relationship between the strain rate and flow stress conforms to the following equations[10,11]:

$$\dot{\epsilon} = A_1 \sigma^k \exp\left(-\frac{Q}{RT}\right). \quad \alpha\sigma \leq 0.5 \quad (4)$$

$$\dot{\epsilon} = A_2 \exp(\beta\sigma) \exp\left(-\frac{Q}{RT}\right). \quad \alpha\sigma \geq 2 \quad (5)$$

$$\dot{\epsilon} = A[\sinh(\alpha\sigma)]^n \exp\left(-\frac{Q}{RT}\right). \quad \alpha\sigma \text{ can take any value} \quad (6)$$

where σ is the flow stress; $\dot{\epsilon}$ is the strain rate; Q is the average apparent activation energy of deformation; R is the ideal gas constant ($R=8.314 \text{ J}\cdot(\text{mol}\cdot\text{K})^{-1}$); T is the deformation temperature; k , A_1 , A_2 , A , α and β are material constants and $\alpha=\beta/k$. Equation (4) and equation (5) are commonly applied to low stress and high stress, respectively. Equation (6) is generally used to describe the flow stress and deformation activation behavior over a wide range of temperature and strain rate. By taking natural logarithm, equation (4) and equation (5) could be written respectively as:

$$\ln \dot{\epsilon} = k \ln \sigma + b_1. \quad (7)$$

$$\ln \dot{\epsilon} = \beta\sigma + b_2. \quad (8)$$

where $b_1 = \ln A_1 - Q/RT$, $b_2 = \ln A_2 - Q/RT$

Fig.3(a) is the linear regression of the relations of $\ln \dot{\epsilon} - \ln \sigma$ at different temperatures. $k=8.000$ could be received as the average slopes of two low stress lines. In a similar way, β can be determined as 0.07364 according to Fig.3(b) and the value of α is $0.009205 \text{ MPa}^{-1}$.

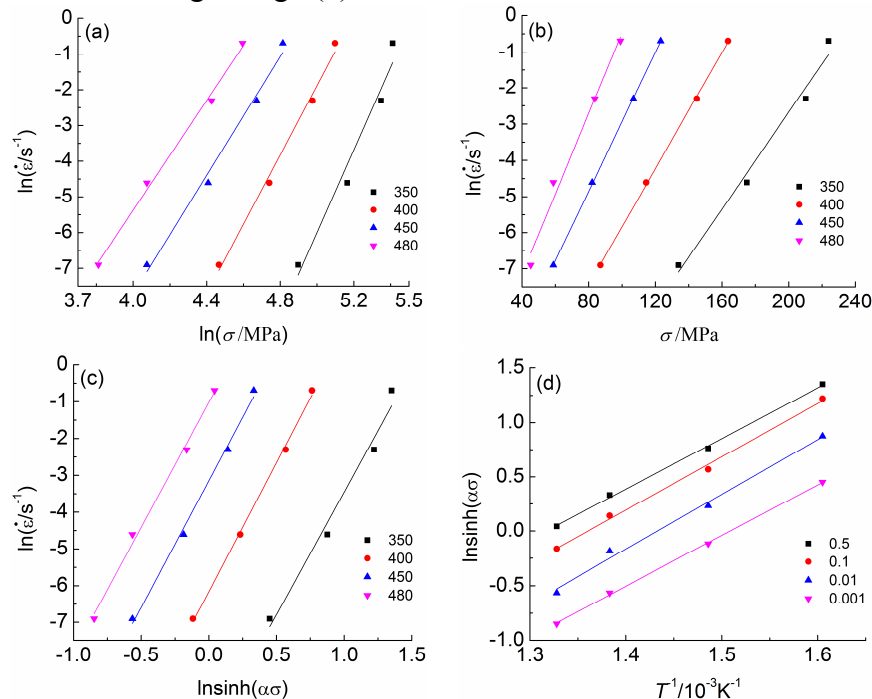


Fig. 3 Relationships between strain rate($\dot{\epsilon}$) and peak stress (σ) and temperatures(T):
(a) $\ln \dot{\epsilon} - \ln \sigma$; (b) $\ln \dot{\epsilon} - \sigma$; (c) $\ln \dot{\epsilon} - \ln[\sinh(\alpha\sigma)]$; (d) $\ln[\sinh(\alpha\sigma)] - 1/T$

equation(6) could be written respectively as equation(9), Q could be written as equation(10)

$$\ln \dot{\epsilon} = n \ln[\sinh(\alpha\sigma)] + b_3. \quad (9)$$

$$Q = Rn \frac{\partial \ln[\sinh(\alpha\sigma)]}{\partial (1/T)}. \quad (10)$$

By average slopes of the four lines of Fig.3(c), n can be determined as 6.8336; Similarly, the value of $\partial \ln[\sinh(\alpha\sigma)]/\partial (1/T)$ is the average slopes of all lines in Fig.3(d), thus the calculated value of Q is obtained to be about $273426 \text{ J}\cdot\text{mol}^{-1}$.

Substituting the values of k , β , α , n , Q in equation(6), the values of A is 3.1788×10^{18} , thus, equation(11) can be described as following

$$\dot{\epsilon} = 3.1788 \times 10^{18} [\sinh(0.009205\sigma)]^{6.8336} \exp\left(-\frac{32887}{T}\right). \quad (11)$$

Fig.4 is the data comparison of model data and actual test data, in which error value is less than 0.055. The model obtained in this experiment can be applied in the temperature range of 623–753 K and strain rates range of 0.001- 0.5 s^{-1} .

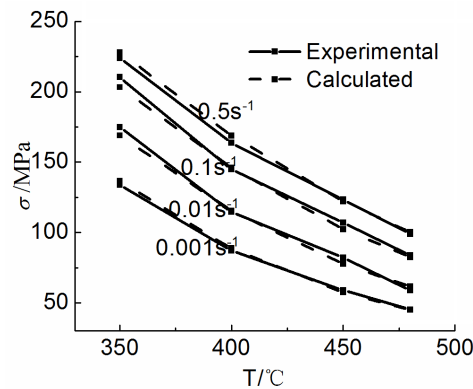


Fig. 4 Comparisons of model data and actual test data

Typical microstructures of the magnesium alloy with pre-homogenization treatment at a strain of 0.7 and at a strain rate of 0.1 s^{-1} at different temperatures are shown in Fig.5.

At all deformation temperatures, almost all of the grains were obviously elongated in the perpendicular direction to the compression axis. The boundaries of elongated grains were nearly straight and no apparent recrystallization grains were observed. At 623 K, the specimen had narrow grains. The grains became wider with increasing temperature. Deformation was the process of competition between work hardening and dynamic softening that happened at the same time. Dynamic softening might be led by deformation heating and also by microstructure instabilities, such as dynamic recovery (DRV), dynamic recrystallization, and texture formation. In this experiment, the important softening mechanisms were eutectic melting and DDRX. From the microstructure of the alloy, we found a lot of eutectic fragments along the grain boundaries and a little DDRX in perpendicular direction to compression axis (Fig.5). This was the reason why grains became thick at elevated temperature. At low temperature, eutectic structure and grain boundaries coalesced well. So the grains were elongated greatly during deformation. At elevated temperature, the eutectic structure became weak and it could be destroyed easily, leaving eutectic fragments. The fragments along the boundaries could turn round so as to take effect of the slippage between grains and the grain structure looked thicker a little[12].